Identification of Glioma Pseudoprogression Based on Gabor Dictionary and Sparse Representation Model

Xiaomei Li[1]*, Gongwen Xu[2], Qianqian Cao[1], Wen Zou[1], Ying Xu[1], Ping Cong[1]

ABSTRACT

This paper aims to find an effective clinical means to separate glioma pseudoprogression from true recurrence. To this end, the sparse representation method was introduced into the field of medical image processing. The key solution is to combine the training samples into a redundant dictionary. With the sparse decomposition algorithm, the test samples were represented by the combination of the sparse linear coefficients of training samples. Then, a suitable classifier was generated for the classification of sparse atoms. Finally, the author carried out a case study and proved that our method can effectively diagnose pseudoprogression in glioma, and enjoys a good prospect of clinical application.

Key Words: Glioma, Radiotherapy (RT), Temozolomide (TMZ) CHEmotherapy, Pseudoprogression, Gabor Dictionary, Sparse Representation Model

DOI Number: 10.14704/nq.2018.16.1.1178 **NeuroQuantology 2018; 16(1):43-51**

Introduction

Malignant gliomas are the most common malignancies of the central nervous system. For glioblastoma and other high-grade gliomas, the standard postoperative treatment often combines radiotherapy (RT) with adjuvant chemotherapy/adjuvant temozolomide (TMZ) chemotherapy (Stupp *et al*., 2005). The treatment efficacy of glioblastoma has been widely evaluated by the McDonald criteria (Macdonald *et al*., 1990), which relies on such imaging indices as baseline and enhanced scan results of the magnetic resonance imaging (MRI). In glioma imaging follow-up, the RT combined with TMZ chemotherapy (RT-TMZ) may cause the enhancement of the original tumour area or the emergence of new enhanced area. The result is called the pseudoprogression related to RT (Taal *et al*., 2008). At present, most scholars attribute such imaging changes to the increased blood-brain barrier permeability due to the treatment or tumour factors (Sanghera *et al*., 2012; Gunjur *et al*., 2011).

According to the literature, the incidence of pseudoprogression falls between 15% and 30% among glioma patients receiving RT-TMZ (Jeon *et al*., 2009). The pseudoprogression, in lack of specific molecular biomarkers, bears high resemblance to tumour recurrence. It is difficult to distinguish the two from each other based on clinical manifestations of patients.

Not even pathological examination, the gold standard for diagnosis, can make a good discrimination of pseudoprogression. The examination requires tissue sampling through stereotactic biopsy or re-craniotomy. Therefore, the procedures are invasive, the sampling sites are very limited, and the patient suffers from

Corresponding author: Xiaomei Li
Address: [1] Department of oncology, the Second Hospital of Shandong University, Jinan 250033, China; [2] School of Business, Shandong Jianzhu University, Jinan 250101, China
e-mail ✉ sdulixiaomei@163.com
Relevant conflicts of interest/financial disclosures: The authors declare that the research was conducted in the absence of any commercial or financial relationships that could be construed as a potential conflict of interest.
Received: 02 November 2017; **Accepted:** 12 January 2018

bodily pain and financial burden.

Radiographic follow-up diagnosis is clinically feasible but not well accepted, for the long follow-up period severely restricts the individualization of treatment options (Chamberlain *et al*., 2007).

To differentiate pseudoprogression from tumour recurrence, many new imaging techniques have been adopted, including MRI diffusion-weighted imaging (DWI), diffusion tensor imaging (DTI) (Knudsen-Baas *et al*., 2013), magnetic resonance imaging (MRS) (Yaman *et al*., 2010), positron emission tomography (PET) (Glaudemans *et al*., 2013), and DSC and arterial spin labelling (ASL) (Choi *et al*., 2013). However, each of these techniques has its own defects, and the effect is yet to be observed.

To sum up, there is still no effective clinical means to separate glioma pseudoprogression from true recurrence. Therefore, this paper aims to find such an identification method considering the change or termination of the treatment plan, as well as the economic condition, living quality and survival rate of the patient.

Routine Diagnostic Methods

Three routine diagnostic methods, namely MRI, MRS and ASL, were adopted for our research. Each of the methods is detailed below.

MRI

The MRI employs the GE Signa HD 1.5T MRI machine with an 8-channel phased-array coil, and T_1- and T_2- weighted imaging (WI). The parameters of 3D FIESTA sequence include: TR 4.6 ms, TE 1.6ms, Flip angle 60°, NEX 6 times, FOV 16cm×16cm, matrix 256×256, block thickness 60mm, and layer thickness 1.0mm. Following the intravenous injection of Gd-DTPA, the axis, coronal plane and sagittal plane were subject to T_1WI enhanced scan.

MRS

The MRS consists of single or multi-voxel H-MRS scans. The single voxel scanning was realized through PRBOE/SV pulse sequence excitation, while the multi-voxel scanning was achieved by point-resolved spectral analysis (PRESS) sequence. The scanning parameters include: TR 1,000ms, TE 35ms, and layer thickness 10mm. The pre-scan was performed automatically for shimming and water suppression.

ASL

The ASL relies on the scanning method of echo planar imaging flow sensitive alternating inversion recovery (EPI FAIR). The scanning parameters include: TR/TE 2,000ms/15ms; T_1 1.2 s; FOV 24cm; matrix 128×128; NEX 100 times; layer thickness 6 mm, number of layers 7, layer spacing 2mm.

After pre-processing and data analysis, the resulting image was transmitted to a GE ADW 4.2 workstation for post-processing. Then, the processed image underwent an MRS enhanced scan to determine the Cho/Cr and NAA/Cr values of the enhanced area and the lesion area.

The FAIR images were used to measure the regional cerebral blood flow (rCBF) within 2cm around the lesion, in the image area and in the lesion, respectively. Then, the measured data were analysed by the imaging physician to determine if there existed pseudoprogression.

In our case, a 45-year-old male patient with astrocytoma in left frontal lobe (WHO Ⅲ grade) received the FR-TMZ after surgery. However, the original symptom in the nervous system got worse. Then, the patient continued with the treatment. Ten months later, the follow-up diagnosis confirmed the existence of pseudo progression.

Figure 1, male, 45 years old. Left precordial lobe astrocytoma (WHO Ⅲ grade) after surgery, combined with temozolomide concurrent chemoradiation January, the original nervous system symptoms worse, continue temozolomide chemotherapy, follow-up 10 months, pseudoprogression was confirmed at last.

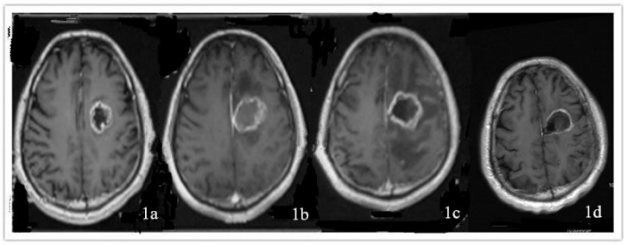

Figure 1. T_1WI enhanced image

1a: there was an unobvious ring-enhancing lesion in the frontal lobe before the operation. 1b: the lesion was enhanced 10 days after surgery. 1c: the lesion was obviously enhanced after the treatment in January. 1d: the lesion was reduced and disappeared 6 months after the treatment.

Sparse Representation

Nowadays, it is a popular trend to combine image processing algorithms and computers in pattern recognition, image processing and biomedicine (Al-Kofahi *et al*., 2010; Aus *et al*., 1986). However, the most intelligent system of image signal processing is still the visual system of human. The visuosensory area in the human brain is a complex, redundant system. For a single signal or stimulus, only a fraction of the related neurons is activated. The information captured by them provides a simple representation of the most basic features of the stimuli to superior sensory nerves. This process is called the sparse representation of the signal in the brain.

Inspired by the visual system, the sparse representation theory has been extensively adopted in every aspect of signal processing, thanks to its low computing load and many other advantages. The theory gives birth to the sparse-land model, which intends to represent the basic information of the signal with the fewest number of nonzero coefficients, thus simplifying the solution to signal processing problems. The model can be expressed as:

$$y=D\alpha, \text{ subject to } \min||\alpha||_0 \quad (1)$$

where $y \in R^n$ is the target signal; $D \in R^{(n \times m)}$ is the basis function dictionary; $\alpha \in R^m$ is the sparse representation vector; $||\alpha||_0 \ll m$ is the sparsity of α, i.e. the number of nonzero coefficients in α (Gao *et al.,* 2010).

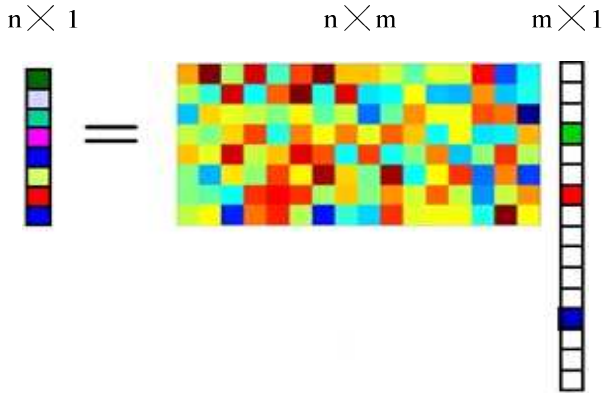

Figure 2. Sparse representation

Recent years has seen the proliferation of the JPEG image format based on discrete cosine transform (DCT) dictionary and the JPEG-2000 image format based on wavelet dictionary. Coupled with these formats, it is possible to construct a sparse representation classifier (SRC) based on sparse representation theory (Wright *et al*., 2009).

The SRC assumes that the test samples can be linearly represented by a sufficient number of training samples, and reconstructed without the contribution from the other samples. In this way, the signal classification problem is transformed to a sparse representation problem.

The SRC is a desirable image classification algorithm. As Wright put it, the SRC is insensitive to data loss, and lowers the importance of feature space selection with sufficiently sparse coefficients. Based on the SRC, Song Xiangfa *et al*. (2012) proposed a multi-label learning algorithm, which makes full use of membership to sort the tags and classify the images. J. Wright *et al.* (2009) developed a robust face recognition method based on the SRC; the method achieved excellent recognition effect in noisy and occluded environments.

In addition, the sparse algorithm has been deeply implemented in medical image processing. For instance, Sun Yubao *et al.* (2009) analysed brain function data by sparse representation. The sparse representation is theoretically mature in the analysis of mini-tumour MRI images (Yu, 2013) and fMRI data (Luo and Puthusserypady, 2005), giving rise to various related algorithms.

The sparse representation theory is suitable for MRI image processing. This is because the MRI images carry special signals with sparse semantic meanings, and the tumour images often contain noise from equipment and human errors (Wan *et al*., 2014). To obtain small residual values and enhance classification effect, the sparse constraint on the solution vector of the object needs to be processed, and then represented by a few atoms in the dictionary. Nevertheless, there is no report on the sparse representation-based identification of the enhanced MRI area after the glioblastoma treatment. Thus, it is very meaningful to find an easy way to timely and accurately differentiate pseudoprogression from recurrence after glioblastoma treatment.

Algorithm Design

To improve the recognition rate of postoperative pseudoprogression and true recurrence of glioma, this section designs a redundant dictionary for the sparse decomposition algorithm, and trains a supervised sparse classification model with numerous postoperative MRI medical images of glioma. The workflow of the sparse

representation-based identification algorithm is illustrated in Figure 3.

First, the test sample should be sparsely represented by atoms based on the redundant dictionary; then, the atoms should be classified to yield the classification results. To this end, the author designed the dictionary and the sparse decomposition algorithm, identified pseudoprogression and recurrence based on the sparse representation model.

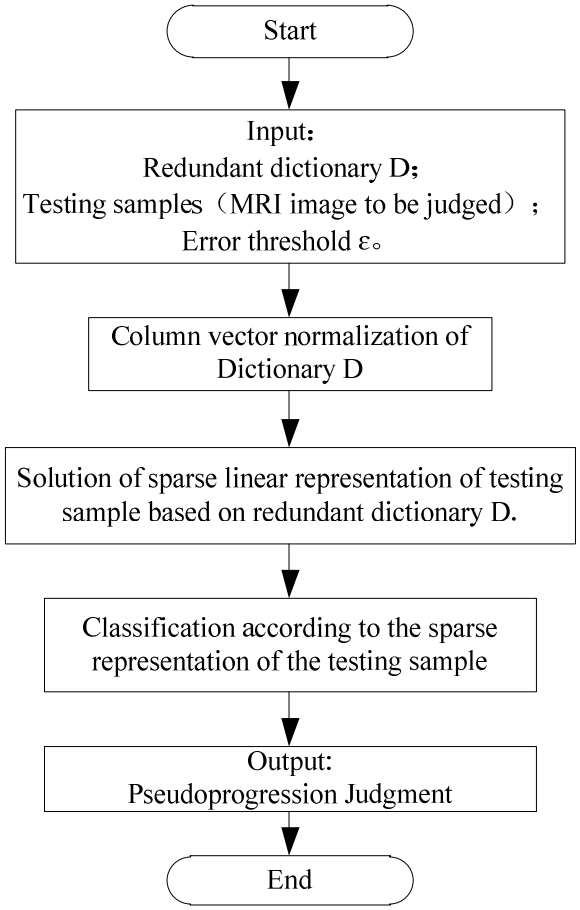

Figure 3. Workflow of the identification algorithm.

Dictionary design

Dictionary design is an important step to sparse representation. The success of sparse representation of MRI images depends entirely on the performance of the dictionary, which in turn relies on the consistency between its atomic structure and internal structure. The consistency is positively correlated with the ease of sparse representation.

In computer vision, traditional dictionaries are adopted for sparse representation. In our research, the dictionaries must be selected properly. For this purpose, redundant dictionaries were learned by training MRI samples of brain tumour patients. Then, a sparse decomposition algorithm for identifying pseudoprogression was designed based on the existing sparse representation theory and sparse decomposition algorithm.

Sparse decomposition algorithm

The process to obtain the optimal sparse representation or sparse approximation of a signal with redundant dictionary is called the sparse decomposition of the signal. This process is essential to the successful application of the sparse representation in MRI image identification. In the case of redundancy, the sparse decomposition of the captured image is an NP-hard problem that requires a combined search and needs to be solved by a suboptimal approximation algorithm. The typical algorithms include relaxation optimization algorithm, greedy tracking algorithm and combinatorial optimization algorithm.

The greedy tracking algorithm mainly selects the atoms for signal decomposition successively from the dictionary by the specific similarity measure. This step is repeated to complete the sparse approximation of the original signal. Compared with the relaxation optimization algorithm, the greedy tracking algorithm does not apply to many practical problems due to its low complexity, high randomness and vulnerability to the local optimum trap.

Greedy matching pursuit algorithm is more effective than the above algorithms in sparse approximation. By this method, the signal is sparsely decomposed by an improved tracking algorithm. The complexity of sparse decomposition mainly depends on the number of atoms in the dictionary. For better efficiency, the image dimension should be reduced, together with the number of atoms in the dictionary.

Sparse representation model

The sparse representation model aims to find a suitable set of basis functions that ensures the sparsity of all MRI images in the training set. With many MRI images as training samples, the basis functions trained by the model will feature spatial locality, directionality and band-pass.

Being a new image processing model, the over-complete image sparse representation offers a concise and convenient way to represent the processed MRI images. In the model, the nonzero coefficient depicts the main structure and essential properties of the MRI images, and the

redundancy system withstands high levels of noises and errors.

Following the sparse representation method, test sample y is linearly represented by the dictionary D. Then, the sparse coefficient vector A is obtained, and the sparseness is used for classification. Ideally, it is assumed that test sample y belongs to class i, and the training samples corresponding to nonzero values in coefficient vector A also belong to class i. This makes it easy to categorize the test sample y into class i. Nevertheless, under the noise influence, some training samples corresponding to some nonzero values in coefficient vector A may fall into other classes. In sparse representation, test sample y is directly classified into the class to which the training sample corresponding to the largest term in the coefficient vector A belongs. Here, the nonzero values of all coefficients in vector A are taken into account.

Hereto, it is possible to identify pseudoprogression and glioma recurrence based on the sparse representation model.

Algorithm Implementation

Training of redundant dictionary

In light of the geometric features of the image and the perception of the human visual system, the 2D Gabor function was selected as the generating function of the multi-component dictionary. The functions of the various free parameters were fine-tuned to create a series of atoms with different scales, directions, aspect ratios, and spatial frequency bandwidths, forming a Gabor perception multi-component dictionary. Based on the geometric features of the image, the sampling density of free parameters was allocated according to the receptive field structure of visual cortex neurons. Thus, the number of atoms in the dictionary was reduced, lowering the complexity of sparse decomposition.

The Gabor function, as a generator of atoms, equals the product of the Gaussian and cosine functions:

$$g(p) = K \exp(-\frac{x^2 + y^2}{}) \cos(2\pi\tau x + \varphi) \quad (2)$$

where p=[x, y] is a discrete image coordinate vector; K is a normalization constant such that $||g||$=1 (L^2 norm); τ is an adjusting factor of oscillation frequency; φ is the cosine phase.

The Gabor perception dictionary was constructed by a series of geometric transformations of the generator functions, which can be expressed as corresponding unitary operators $U(\gamma)$. Thus, the Gabor perception dictionary can be expressed as:

$$D = \{U(\gamma)g, \gamma \in \Gamma\} \quad (3)$$

where γ is an indicator of transformation parameters; Γ is an indicator set.

In general, the dictionary is constructed through the following transformations:

1. Move atom α to any position in the discrete image;
2. Rotate θ to match atoms in different directions on contour edge and in texture structure;
3. Perform anisotropic scaling s=(s_1, s_2) so that atoms can match the anisotropic structure of the contour.

Through the above steps, it is possible to match the geometry at different positions, orientations and dimensions in an image.

Therefore, the geometric transformation $U(\gamma)$ of the generated function g can be decomposed as:

$$U(\gamma)\, g = H(\alpha, \theta)\, S(s_1, s_2)\, g \quad (4)$$

where H is the Euclidean transformation group:

$$H(b, \theta)\, g(p) = g(r_\theta(p - \alpha)) \quad (5)$$

where $r_\theta = \begin{pmatrix} \cos\theta & -\sin\theta \\ \sin\theta & \cos\theta \end{pmatrix}$ is a rotation matrix; S is an anisotropic telescoping operator.

$$S(s_1, s_2)g(\vec{p}) = \frac{1}{\sqrt{s_1 s_2}} g(\frac{x}{s_1}, \frac{y}{s_2}) \quad (6)$$

Thus, a structured Gabor dictionary was constructed after the generated functions underwent a series of geometric transformations. Each atom in the dictionary can be measured by the set of geometric transformation parameters γ, which includes moving α, rotation θ, and anisotropic scaling S.

Finally, each atom in the dictionary can be expressed as:

$$g_\gamma(x,y) = K\exp(-\frac{x'^2+y'^2}{2})\cos(2\pi\tau x'+\varphi) \quad (7)$$

$$x' = \frac{\cos\theta(x-\alpha_1)+\sin\theta(y-\alpha_2)}{s_1} \quad (8)$$

$$y' = \frac{\cos\theta(y-\alpha_2)-\sin\theta(x-\alpha_1)}{s_2} \quad (9)$$

The Gabor atoms of different structures form an optimal response to the image content. The response reflects the exact scale, orientation, centre position, phase, and structure of the image. With the transformation parameters, the Gabor atoms can display different number of stripes, scales, aspect ratios, directions, and morphologies. Therefore, these atoms are more than capable of representing the edge contour or texture of different scales, aspect ratios and directions in the MRI image structure. Note that the dictionary can achieve better sparse representation thanks to the anisotropy and multi-directions of the atoms. The combinations of free parameters generate different sub-component dictionaries, which together form the multi-component dictionary.

Implementation of sparse decomposition algorithm

Based on redundant dictionary, the sparse representation itself is an NP-hard problem. As mentioned above, the typical signal approximation methods for sparse representation include relaxation optimization algorithm, greedy tracking algorithm and intelligent optimization algorithm. In addition, the greedy matching pursuit is a popular, low complexity sparse decomposition algorithm.

The sparse decomposition algorithm was designed as follows. Taking the inner product as a measure of correlation, the atom most relevant to the residual signal was adopted at the selection of any dictionary $D=\{\phi_\gamma \mid ||\phi_\gamma||=1, \gamma\in\Gamma\}$. This step was repeated to gradually approximate the MRI image.

The specific steps of the algorithm are as follows:

1. Let the initial residual signal be the original signal $R^0f=f$, and the initial number of iteration $i=0$;
2. Calculate the inner product coefficient of the residual signal R^if and all the atoms $\alpha_\gamma = \langle R^if, \phi_{\gamma\in\Gamma}\rangle$ in the dictionary;
3. Search for the maximum inner product $\gamma_i = \arg\max_{\gamma\in\Gamma}|\alpha_\gamma|$, and record atomic subscripts γ_i and coefficients $\alpha\gamma_i$;
4. Update the residual signal $R^{i+1}f=R^if-\alpha_{\gamma i}\gamma_i$;
5. If the residual signal energy is less than the given threshold ξ_{stop}: $||R^{i+1}f||^2 \le \xi_{stop}$, terminate the iteration; otherwise, $i=i+1$ and go to Step 2.

After N iterations, the signal f can be sparsely decomposed into:

$$f = \sum_{i=0}^{N-1}\alpha_{\gamma_i}\phi_{\gamma_i} + R^Nf \quad (10)$$

As N approaches infinity, the finite dimensional signal space $||R^Nf||$ converges exponentially, $\lim_{N\to\infty}\|R^Nf\| = 0$. Correspondingly, the obtained signal is decomposed into

$$f = \sum_{i=0}^{+\infty}\alpha_{\gamma_i}\phi_{\gamma_i} \quad (11)$$

The matching pursuit algorithm iteratively looks for Gabor atoms in the dictionary that best match the image structure, aiming to depict the accurate position, scale, direction, amplitude, phase, frequency and other features of the edge and texture in the MRI image.

Establishment of sparse representation model

As mentioned above, test sample y in sparse representation is directly classified into the class to which the training sample corresponding to the largest term in the coefficient vector A belongs. Here, the nonzero values of all coefficients in vector A are taken into account.

In sparse decomposition, the objective function optimization is the same as the Lasso problem. The solution to the Lasso model is depicted below:

Suppose there is a linear regression model with M observed data for K predictors in its dataset. Let $Y=(y_1, y_2, \ldots, y_n)^T$ be the measured variables, and $X_j=(x_{1j}, x_{2j}, \ldots, x_{nj})^T$ (j=1,2,…,K) be the types of predicted data.

After both X_j and Y are normalized, the Lasso problem becomes a least squares problem with l_1 norm penalties.

Hence, the solution to the Lasso model translates to solving the optimization problem below:

$$\alpha_{Lasso} = \min_{\alpha} \left\| Y - \sum_{j=1}^{K} x_j \alpha_j \right\|_2^2 + \lambda \left\| \sum_{j=1}^{K} \alpha_j \right\|_1 \quad (12)$$

where λ in is a non-negative parameter. The Laaso model at once guarantees the accuracy and sparseness of the system, and is applicable to the variable selection of MRI images.

The SRC classification algorithm:

1. Input: Training sample matrix of K sample classes

$$A = \left[A_1, A_2, \ldots, A_k \right] \in R^{m \times N}.$$

Test sample $y \in R^m$; error tolerance: $\varepsilon > 0$.

2. Perform l_2 norm regularization of the column vector of sample matrix A.

3. Solve the l_1 minimization problem:

$$\alpha_1 = \min_{\alpha} \|\alpha\|_1 \; s.t. \; \|y - A\alpha\|_2 \le \varepsilon$$

4. Calculate each class residual:

$$r_i(y) = \|y - A\delta_i(\alpha_i)\|_2 \quad i = 1, 2, \ldots, K$$

5. Output: Test sample y belongs to the sample class with the smallest residual $r_i(y)$.

The sparse representation coefficients α contain important information to determine whether the test sample belongs to the training set: If yes, the coefficients α have good sparsity, and the nonzero elements are mainly concentrated in one sample class; otherwise, the coefficients α are distributed across multiple sample classes and definitely not sparse. Therefore, a sparse concentration index (SCI) was defined to measure the concentration of coefficients in a sample class:

$$SCI(\alpha) = \frac{k \cdot \max_i \left\| \delta_i(\alpha) \right\|_1 / \left\| \alpha \right\|_1 - 1}{k - 1} \in [0, 1] \quad (13)$$

The α can be obtained by the SRC algorithm. If $SCI(\alpha_i)=1$, the test sample can be accurately represented by training a certain sample class; If $SCI(\alpha_i)=0$, the test sample is uniformly distributed across the sample classes, and cannot be represented by one sample alone.

Hence, $\tau \in [0, 1]$ was set as the threshold for acceptable test samples. If $SCI(\alpha_i) \geq \tau$, the test sample belongs to the pseudoprogression training set; otherwise, the test sample is not valid.

Results

The research data were collected from 362 patients (males: 218; females: 144; age: 19~70; medium age: 50) who received high-grade glioma surgery and postoperative RF-TMZ between January 2014 and December 2016 in several hospitals. One month after the surgery, enhanced lesion area appeared on their MRI images.

The Karnofsky performance score (KPS) ranged from 70 to 90, putting the medium score at 80. All patients were confirmed as tumour-stricken. Among them, 193 cases fell to WHO grade III (i.e. anaplastic astrocytoma, ameloblastoma, and atypical oligodendroglioma) and 169 to WHO grade IV (glioblastoma).

According to the pathologic analysis after the second surgery and the 10-month follow-up diagnosis, 283 of the 362 cases were confirmed as pseudoprogression, and 79 as tumour recurrence. In 283 cases of pseudoprogression, 124 cases were confirmed by the pathologic analysis after the second surgery, and 159 cases were confirmed by the 10-month follow-up diagnosis. In 79 cases of tumour recurrence, 63 cases were confirmed by the pathologic analysis after the second surgery, and 16 cases were confirmed by the 10-month follow-up diagnosis.

By the MRS analysis method, 198 cases were diagnosed as pseudoprogression, and 164 as tumour recurrence. According to the pathologic analysis after the second surgery and the 10-month follow-up diagnosis, 188 of the 198 cases were confirmed as pseudoprogression, and 10 as tumour recurrence; 95 of the 164 cases were confirmed as pseudoprogression, and 69 as tumour recurrence.

By the ASL analysis method, 247 cases were diagnosed as pseudoprogression, and 115 as tumour recurrence. According to the pathologic analysis after the second surgery and the 10-month follow-up diagnosis, 231 of the 247 cases were confirmed as pseudoprogression, and 16 as tumour recurrence; 52 of the 115 cases were confirmed as pseudoprogression, and 63 as tumour recurrence.

By our method, 275 cases were diagnosed as pseudoprogression, and 87 as tumour recurrence. According to the pathologic analysis

after the second surgery and the 10-month follow-up diagnosis, 268 of the 275 cases were confirmed as pseudoprogression, and 7 as tumour recurrence; 15 of the 87 cases were confirmed as pseudoprogression, and 72 as tumour recurrence. Through comparison, it is clear that our method achieved higher recognition rate of pseudoprogression than the MRS and the ASL methods. Moreover, the proposed method boasts a great application potential, as it depends on machine learning rather than doctor's experience

Conclusion

To accurately differentiate pseudoprogression from glioma recurrence, this paper establishes a sparse representation model that can promptly formulate individualized treatment plans, select a reasonable treatment plan for each patient, and accurately evaluate the treatment effect.

Therefore, the sparse representation method was introduced into the field of medical image processing. The key solution is to combine the training samples into a redundant dictionary. With the sparse decomposition algorithm, the test samples were represented by the combination of the sparse linear coefficients of training samples. Then, a suitable classifier was generated for the classification of sparse atoms. In the end, a case study was carried out to show that the proposed method can accurately distinguish glioma pseudoprogression from tumour recurrence.

The method allows early detection of and intervention in glioma, and reduces the economic and physical stress on patients with pseudoprogression.

Acknowledgement

This work was supported in part by the Key Research and Development Foundation of Shandong Province (2016GGX101035), the Development Projects of Science and Technology of Jinan (201602151), the Second Hospital of Shandong University Youth Research Fund(S2015010004), and Shandong Soft Science Research Planning Project (2017RKB01077).

References

Al-Kofahi Y, Lassoued W, Lee W. Improved automatic detection and segmentation of cell nuclei in histopathology images. IEEE Transactions on Biomedical Engineering 2010;5(4):841-52.

Aus HM, Harms H, Haucke M. Leukemia-related morphological features in blast cells. Cytometry 1986; 7(4):365-370.

Chamberlain MC, Glantz MJ, Chalmers L, Van Horn A, Sloan AE. Early necrosis following concurrent Temodar and radiotherapy in patients with glioblastoma. Journal of neuro-Oncology 2007; 82(1):81-83.

Choi YJ, Kim HS, Jahng GH, Kim SJ, Suh DC. Pseudoprogression in patients with glioblastoma: added value of arterial spin labeling to dynamic susceptibility contrast perfusion MR imaging. Acta Radiologica 2013; 54(4):448-54.

Da Cruz LH, Rodriguez I, Domingues RC, Gasparetto EL, Sorensen AG. Pseudoprogression and pseudoresponse: imaging challenges in the assessment of posttreatment glioma. American Journal of Neuroradiology 2011; 32(11):1978-85.

Gao SH, Tsang IWH, Chia LT. Kernel Sparse Representation for Image Classification and Face Recognition. Lecture Notes in Computer Science 2010; 63(14):1-14.

Glaudemans AW, Enting RH, Heesters MA, Dierckx RA, van Rheenen RW, Walenkamp AM, Slart RH. Value of 11C-methionine PET in imaging brain tumours and metastases. European Journal of Nuclear Medicine and Molecular İmaging 2013; 40(4):615-35.

Gunjur A, Lau E, Taouk Y, Ryan G. Early post-treatment pseudo-progression amongst glioblastoma multiforme patients treated with radiotherapy and temozolomide: A retrospective analysis. Journal of Medical İmaging and Radiation Oncology 2011; 55(6):603-10.

Jeon HJ, Kong DS, Park KB, Lee JI, Park K, Kim JH, Kim ST, Lim DH, Kim WS, Nam DH. Clinical outcome of concomitant chemoradiotherapy followed by adjuvant temozolomide therapy for glioblastaomas: single-center experience. Clinical Neurology and Neurosurgery 2009;111(8):679-82.

Knudsen-Baas KM, Moen G, Fluge Ø, Storstein A. Pseudoprogression in high-grade glioma. Acta Neurologica Scandinavica 2013; 127(s196): 31-37.

Luo H, Puthusserypady S. A sparse Bayesian method for determination of flexible design matrix for fMRI data analysis. IEEE Transactions on Circuits and Systems I: Regular Papers 2005; 52(12):2699-2706.

Macdonald DR, Cascino TL, Schold Jr SC, Cairncross JG. Response criteria for phase II studies of supratentorial malignant glioma. Journal of Clinical Oncology 1990; 8(7): 1277-80.

Sanghera P, Rampling R, Haylock B, Jefferies S, McBain C, Rees JH, Soh C, Whittle IR. The concepts, diagnosis and management of early imaging changes after therapy for glioblastomas. Clinical Oncology 2012; 24(3): 216-27.

Song X, Jiao L. A Multi-Label Learning Algorithm Based on Sparse Representation. Pattern Recognition and Artificial Intelligence 2012; 25(1):124-29.

Stupp R, Mason WP, Van Den Bent MJ, Weller M, Fisher B, Taphoorn MJ, Belanger K, Brandes AA, Marosi C, Bogdahn U, Curschmann J. Radiotherapy plus concomitant and adjuvant temozolomide for glioblastoma. New England Journal of Medicine 2005; 352(10): 987-96.

Sun Y, Wu M, Wei Z, Xiao L, Feng C. EEG Spike Detection Using Sparse Representation. Acta Electronica Sinica 2009; 37(9):1971-78.

Taal W, Brandsma D, de Bruin HG, Bromberg JE, Swaak-Kragten AT, Sillevis Smitt PAE, van Es CA, van den Bent MJ. Incidence of early pseudoprogression in a cohort of malignant glioma patients treated with chemoirradiation with temozolomide. Cancer 2008; 113(2):405-10.

Wan SY, Wang X, He S, Wang C. Brain tumor segmentation based on morphological multi-scale modification. Journal of Computer Applications 2014; 34(2):593-96.

Wright J, Yang AY, Ganesh A, Sastry SS, Ma Y. Robust face recognition via sparse representation. IEEE Transactions on Pattern Analysis and Machine İntelligence 2009; 31(2):210-27.

Yaman E, Buyukberber S, Benekli M, Oner Y, Coskun U, Akmansu M, Ozturk B, Kaya AO, Uncu D, Yildiz R. Radiation induced early necrosis in patients with malignant gliomas receiving temozolomide. Clinical Neurology and Neurosurgery 2010;112(8):662-67.

Yu X. The Research of Brain Tumor Image Processing Based on Sparse Representation Model. Anhui University 2013; 5:6-11.